#### **ORIGINAL PAPER**





# Elucidating photophysics-photochemistry relationship in singlet fission materials

Winston T. Goldthwaite<sup>1</sup> · Michael O. Chase<sup>1</sup> · Madalyn R. Gragg<sup>1</sup> · Roshell Lamug<sup>1</sup> · Dean Windemuller<sup>2</sup> · Sean Parkin<sup>2</sup> · John E. Anthony<sup>2</sup> · Oksana Ostroverkhova<sup>1</sup>

Received: 21 November 2023 / Accepted: 2 February 2024 © The Author(s), under exclusive licence to The Materials Research Society 2024

#### **Abstract**

Photodegradation poses a significant challenge in organic optoelectronic devices; understanding its relationship with photophysics is necessary for optimizing optoelectronic performance and photostability. We study such relationship in singlet fission (SF) materials TIPS-Pentacene (TIPS-Pn) and tetracene derivatives (R-Tc) with different morphologies. We explore how photochemistry can promote understanding of intermolecular processes such as SF through the evolution of excited states during photodegradation. Photoluminescence emission competitive to SF experiences a large increase in yield during photodegradation as SF pathways are disabled from either endoperoxide formation (in air) or photodimerization (without air) degradation processes. We observe morphology-dependent photodimerization in TIPS-Pn films and R-Tc crystals and multiple emissive states in R-Tc crystals. The 'slip-stack' packing motif in R-Tc crystals favors formation of emissive trap states and promotes photodimerization. In strong external magnetic fields that suppress SF in R-Tc, enhanced photodimerization is observed, which suggests that morphologies conducive to triplet pair separation could reduce photodimerization.

### Introduction

Photodegradation is one of the major obstacles in the application of organic semiconductors in devices such as fieldeffect transistors, light-emitting diodes, and photovoltaic cells. Functionalized acenes are benchmark (opto)electronic materials, which have high-charge carrier mobility, photoconductivity, and efficient singlet fission [1, 2]. However, these materials are susceptible to photodegradation via reactions with oxygen and photodimerization [3–5], and the quest for molecular design of more stable acenes remains open. Singlet fission is a spin-allowed conversion of a singlet exciton (S<sub>1</sub>) into two triplet excitons (T<sub>1</sub>), S<sub>0</sub>+S<sub>1 $\rightarrow$ </sub><sup>1</sup>(TT) (T..T)  $T_1+T_2$ , where the triplet pair  ${}^1(TT)$  is an intermediate state, which is delocalized across neighboring molecules and (T..T) denotes partially separated triplet pairs that maintain spin coherence [6]. Singlet fission could enable higher theoretical charge conversion efficiency than that in current

devices, potentially helping surpass the Shockley–Queisser limit for silicon solar cells [7]. The efficiency of <sup>1</sup>(TT) formation and separation into free triplet excitons depends on the molecular structure and packing [8]. This prompts the need for designing molecules with structure and packing motifs that are optimized for both highly efficient singlet fission and low photodegradation, which motivates our study of photophysics side by side with photochemistry in selected functionalized acenes.

In this article, we study the photodegradation of benchmark singlet fission material TIPS-Pentacene (TIPS-Pn) and functionalized tetracene derivatives (R-Tc) with different packing motifs dictated by side groups R (Fig. 1). We investigate the photodegradation mechanisms of endoperox-

ide (EPO) formation and photodimerization and their impact on optical and electronic properties. We also explore how photochemistry responsible for degradation could provide insight into intermolecular processes such as singlet fission and elucidate the excited states involved.

Published online: 28 February 2024



<sup>♦</sup> Oksana Ostroverkhova oksana@science.oregonstate.edu

Department of Physics, Oregon State University, Corvallis, OR 97331, USA

Department of Chemistry, University of Kentucky, Lexington, KY 40511, USA

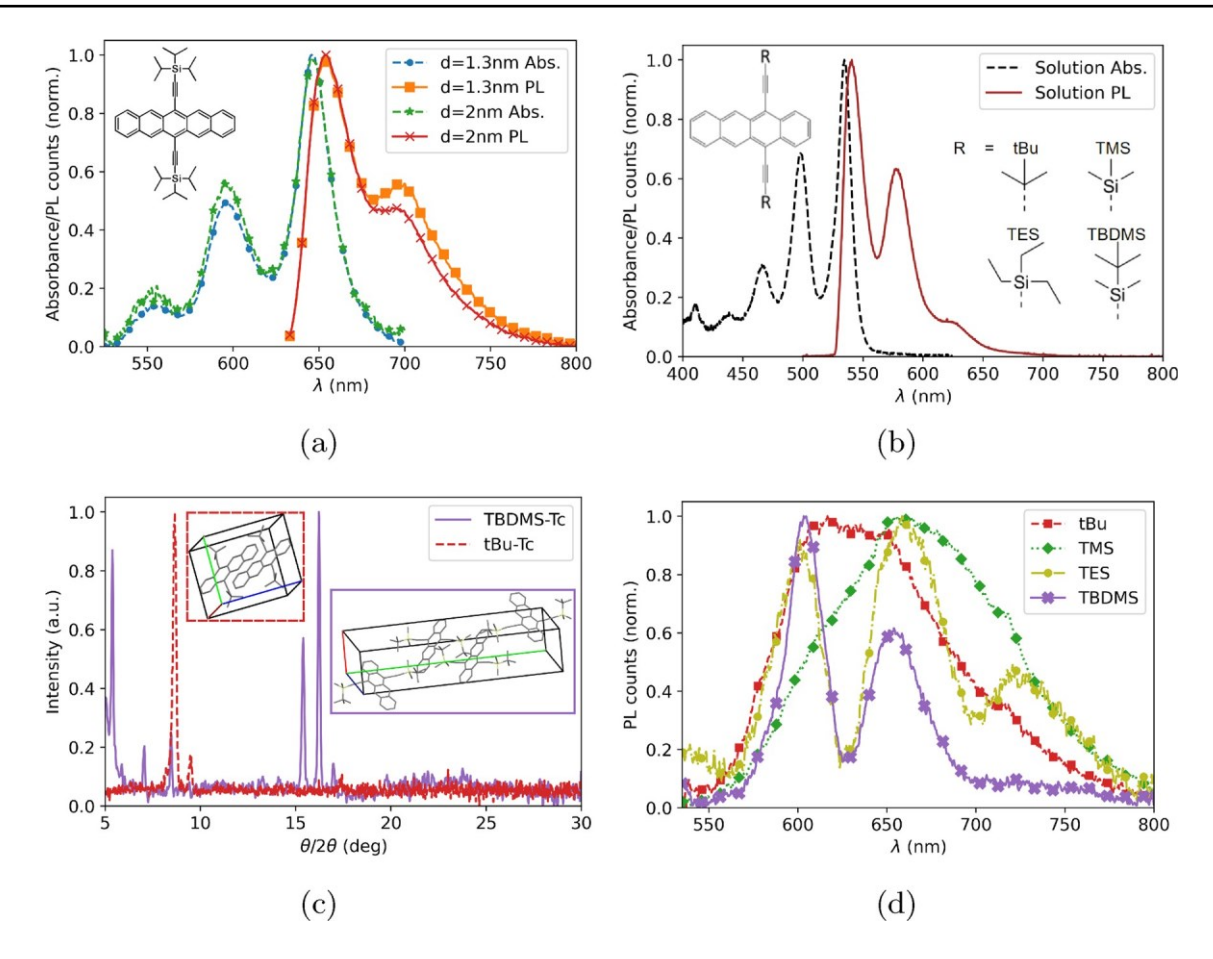


**Fig. 1** a Absorption and PL spectra of TIPS-Pn:PMMA thin films (d = 1.3 nm and d = 2 nm), inset: TIPS-Pn molecular structure. **b** Absorption and PL spectra of dilute TES-Tc solution, representative of R-Tc (R = TMS, TBDMS) monomer behavior; tBu-Tc spectra are blue-shifted by 7 nm (data not shown). Insets: molecular structures of R-Tc and the side groups R. **c** XRD of tBu-Tc and TBDMS-Tc crys-

talline samples on glass/Ag substrates. The tBu-Tc is representative of 'slip-stack' packing shared by TMS- and TES-Tc, whereas TBDMS-Tc has 'sandwich-herringbone' packing (inset). **d** PL spectra of fresh (i.e., before photodegradation) R-Tc crystals, with several emissive states exhibited by R-Tc derivatives

### **Methods**

### Materials and sample preparation

TIPS-Pn solutions were prepared in toluene with poly(methyl methacrylate) (PMMA) in different concentrations to yield TIPS-Pn:PMMA films with average intermolecular distances (d) between TIPS-Pn molecules of d = 1.3 nm and d = 2 nm as described in [9]. Two sample configurations were utilized (Fig. 2): the 'bottom' sample, where a 45 nm silver (Ag) mirror was deposited onto a glass substrate and the solution was spincast onto the mirror, or the 'top' sample, where the solution was spincast onto the glass substrate and the mirror was deposited on top of the thin film to protect it from oxygen.

To form R-Tc crystals, 3-5 mM R-Tc solutions in toluene or chlorobenzene were deposited onto a substrate

in a 0 ° C chiller and let slowly evaporate, resulting in multiple R-Tc crystals; X-ray diffraction data from a collection of such crystals for TES-Tc and TBDMS-Tc are included in Fig. 1c. XRD data were taken using a Rigaku SmartLab in a o/2o geometry with a wavelength of 1.54 Å . Crystals were deposited either onto a glass substrate and capped with a 45 nm Ag layer (similar to the 'top' samples described above) for optical measurements or on a glass substrate patterned with 80/10 nm-thick Au/Cr interdigitated electrodes with 25  $\mu$ m spacing for electrical characterization. The latter samples were then capped with a 25 nm layer of  $Si_3N_4$  to prevent the crystals from oxidizing.

Crystals of four R-Tc derivatives, with two packing motifs, were explored: R-Tc with R= tBu, TMS, and TES groups (inset of Fig. 1b) have a 'slip stack' packing with different 'slip' and intermolecular spacing, and TBDMS-Tc has 'sandwich-herringbone' structure (inset of Fig. 1c). The

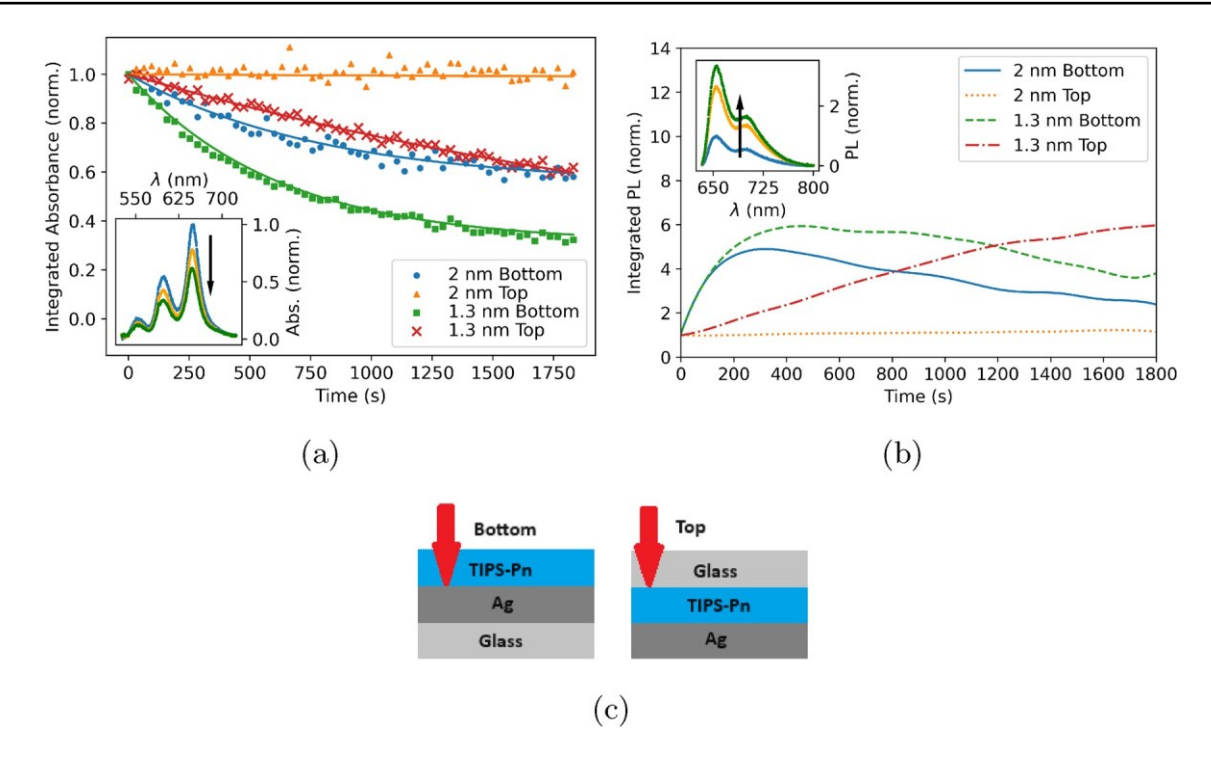


**Fig. 2** a Integrated  $S_0$ - $S_1$  absorbance of TIPS-Pn:PMMA films with d=1.3 and 2 nm, in 'top' and 'bottom' samples, during photodegradation under 633 nm cw excitation at 20 W/cm². Single-exponential fits to the data are also included. Inset shows spectral evolution of absorbance during photodegradation of TIPS-Pn:PMMA d=1.3 nm 'bottom' sample. **b** Integrated PL of TIPS-Pn during photodegradation under 150 W/cm² 633 nm excitation, where the d=2 nm

'bottom' and both d=1.3 nm samples have a large increase in PL yield as they degrade via EPO formation ('bottom' samples) and photodimerization ('top' samples). Inset shows spectral evolution of PL in TIPS-Pn:PMMA d=1.3 nm 'bottom' sample during photodegradation via EPO formation. c Schematics of 'bottom' and 'top' sample configurations; arrow depicts excitation direction

side groups R have different volume (tBu:  $100 \text{ Å}^3$ , TMS: 109Å, TES: 151 Å, TBDMS: 156 Å, which contributes to limits on the nearest intermolecular distance. These volumes were determined with DFT calculations using Gaussian 16 Rev A.03. Geometry optimizations (wB97XD/6-31 G\*) were performed with solvent modelled using a polarizable continuum model (PCM). The PCM is an implicit solvation model where solvent molecules are approximated as spheres with size and polarity according to the chosen solvent. The calculated volume that does not contain solvent particles is taken to be the volume of the side chain. The three 'slipstack'-packing crystals have Z=2 unit cells with lattice constants: tBu-Tc **a**=9.6 A, **b**=10.6 A, **c**=11.8 A; TMS-Tc a=11.1 A, b=11.5 A, c=12.1 A; and TES-Tc a=11.8 A,  $\mathbf{b}$ =12.4 A,  $\mathbf{c}$ =13.2 A. TBDMS-Tc has a Z=4 unit cell with **a**=6.9 A, **b**=32.7 A, **c**=13.3 A.

### **Measurements**

For optical absorption measurements, samples were illuminated by a tungsten halogen lamp focused onto the sample with a 20x objective. Reflected light was collected

and analyzed with a fiber-coupled OceanOptics USB2000 spectrometer. Photoluminescence (PL) was measured using continuous wave (cw) 633 nm HeNe laser excitation for TIPS-Pn and 532 nm Nd:YVO<sub>4</sub> laser (Verdi-5, Coherent, Inc.) excitation for R-Tc. The excitation beam was focused on the sample and the PL was collected as in measurements of absorption, using a 633 nm or 532 nm long-pass (LP) filter.

Select TES- and TBDMS-Tc crystal samples were placed in a magneto-optic cryostat (OptiCool, Quantum Design, Inc.) for magnetic-field- (B-field) dependent measurements. PL was measured with 532 nm cw excitation focused with a 10x objective to a near diffraction-limited spot (<5  $\mu$ m) on a single crystal. The PL was collected in reflection and measured using a SpectraPro HRS-300 spectrograph after filtering the excitation beam with a 532 nm LP filter.

For photocurrent measurements, the samples were illuminated with a 532 nm cw laser. Voltage was applied, and the current–voltage and current-time (using modulated laser excitation) characteristics in the dark and under illumination were measured using a Keithley 237 source-measure unit. The photocurrent was calculated by subtracting the dark current from the current under illumination after 10 s of

light exposure. The dark current was measured as the current before each period of light exposure.

To measure evolution of optical and electronic properties during photodegradation, the sample was continuously exposed to the 633 nm or 532 nm laser for TIPS-Pn and R-Tc, respectively, to induce photodegradation. Absorption and PL spectra were measured periodically over time to track the evolution of these properties as the sample undergoes chemical reactions. For the photocurrent degradation measurements, the sample was continuously illuminated with a 532 nm laser for 1, 2, 3, or 4 min; after each illumination cycle, the sample was kept in the dark for 1 min, after which the light was turned on and the current under illumination was measured after 10 s of light exposure. The photocurrent was calculated by subtracting the dark current, immediately preceding illumination, from the current under illumination.

### **Results**

Optical absorption and PL spectra of fresh (i.e., before photodegradation) samples are shown in Fig. 1. In dilute solution, both TIPS-Pn and R-Tc (TES-Tc shown) absorption and PL spectra are vibronic progressions due to the excitation coupling to C–C stretching modes [10]. The S<sub>0</sub>-S<sub>1</sub> 0–0 absorption exhibits peaks at 647, 534, and 527 nm in TIPS-Pn, R-Tc (R= TES, TMS, TBDMS), and tBu-Tc, respectively, and the Stokes shifts are below 10 nm.

TIPS-Pn:PMMA film with d=2 nm exhibits absorption spectrum similar to that of solution; the more concentrated TIPS-Pn:PMMA d=1.3 nm film has both amorphous and crystalline domains [9], with the absorption spectra of amorphous domains matching those of the d=2 nm film (Fig. 1a). Both TIPS-Pn:PMMA films emit only from the  $S_1$  state with the solution-like 0-0 peak at 660 nm followed by a vibronic progression. This emission originates from molecules in domains with morphology unfavorable for singlet fission, which is the dominant process that quenches PL in TIPS-Pn films. The emission from the TIPS-Pn:PMMA d=1.3 nm film is considerably reduced as compared to that from the d=2 nm film, due to a more efficient singlet fission in more concentrated films, as reported in our previous study [9].

Similar to other functionalized acenes [10, 11], R-Tc (R = TES, TMS, TBDMS) dilute solution spectra are unaffected by side groups R. In crystals, however, the side groups have a large impact on the morphology, and crystalline R-Tc has significantly different photophysics depending on the molecular packing. These effects are apparent in the PL, as shown in Fig. 1d, with a range of emissive states in the 590-720 nm range, red-shifted from the  $S_1$  0-0 emission in solutions at 540

nm. The emission with a dominant peak centered at 600 nm, present in PL from all derivatives, will be referred to as  $S_{lagg}$  emission from molecular aggregates [12]. Emission maximized at >630 nm in TES-, TMS-, and tBu-Tc is attributed to low-energy trap states [13] and will be referred to as Sx emission. At room temperature, both the  $S_{lagg}$  and Sx emission were weak (<10% quantum yield) in all crystals under study, as most of the initial excitation populates dark  $^{1}(TT)/T$ ..T states in the process of singlet fission.

# TIPS-Pn:PMMA films: photophysics vs photochemistry

To study the effects of photodegradation, both absorbance and PL of TIPS-Pn:PMMA films were measured as the sample was continuously illuminated with a 633 nm light [14]. Qualitatively similar behavior was observed in both 'bottom' and 'top' samples: the total S<sub>0</sub>-S<sub>1</sub> absorbance decreased, while the S<sub>1</sub> PL increased over time, with no new absorption or PL from photodegradation products observed in the spectral range under study (Fig. 2). Inset of Fig. 2a shows the evolution of TIPS-Pn:PMMA d = 1.3 nm film absorption in the 'bottom' sample configuration (Fig. 2c). The S<sub>0</sub>-S<sub>1</sub> absorption of TIPS-Pn decreased, which we attribute to the EPO formation, the dominant photodegradation process when the TIPS-Pn molecules are exposed to oxygen in air [3]. The molecules in films in the 'top' configuration, which minimizes oxygen exposure (Fig. 2c), degraded considerably slower, via photodimerization, most likely forming a 'butterfly' dimer [4]. Both EPOs and 'butterfly' dimers have significantly blue-shifted spectral features as compared to parent TIPS-Pn molecules and do not contribute to absorption or emission in the >530 nm range under study. Therefore, the observed initial increase in PL during the photodegradation is due to degradation of one of the molecules in the molecular pairs that undergo singlet fission, which enhances PL from the remaining molecules that are still intact. Figure 2a shows integrated S<sub>0</sub>-S<sub>1</sub> absorbance, normalized at its value at t = 0, vs illumination time (t) of TIPS-Pn:PMMA d = 1.3nm and d = 2 nm films in both sample configurations. To compare the photodegradation rate constants (k), the data were fitted by a single-exponential decay ( $\sim e^{-kt}$ ). For the 'bottom' samples these fits yield  $k=(1.3 \pm 0.1) \cdot 10^{-3} \text{ s}^{-1}$  for the d = 2 nm film and  $k=(1.6 \pm 0.1) \cdot 10^{-3} \text{ s}^{-1}$  for the d = 1.3 nm film. The d = 1.3 nm 'top' sample had a degradation rate constant of  $k=(3.3 \pm 0.6) \cdot 10^{-4} \,\mathrm{s}^{-1}$ , indicating that in the d = 1.3 nm samples, under the same excitation conditions, EPOs formed with a rate constant about five times higher than photodimers. In the d = 2 nm 'top' sample, minimal photodimerization occurred under our illumination conditions, consistent with the relatively large average intermolecular

distance reducing the number of neighboring molecules in configurations favorable for photodimerization.

The integrated PL vs time upon continuous 633 nm light illumination for the same samples is shown in Fig. 2b. Initially, the S<sub>1</sub> emission increases (inset of Fig. 2b) as the sample is illuminated, increasing the total PL yield over time. This growth in PL yield, which was observed both in 'bottom' and 'top' samples, indicates that photodegradation via either EPO formation or photodimerization is disabling a competitive process by destroying the molecules participating in the singlet fission (i.e. those in dark <sup>1</sup>(TT)/ T..T states). This leads to a greater population of molecules that are unable to undergo singlet fission and relax via emission instead. In the 'bottom' samples, the PL yield reaches maximum (at factors of 5 and 6 higher emission than that from the fresh samples with the d = 2 and 1.3 nm, respectively) followed by a decrease as the rest of the molecules reacts with oxygen to form the EPOs. In the 'top' samples, the PL yield increases for the duration of the measurement, reaching a level higher by a factor of 6 than that from the

fresh sample with d=1.3 nm, as molecules in the dark states slowly dimerize, inhibiting singlet fission and increasing  $S_1$  PL. The photodimerization in the sample with d=2 nm is considerably reduced, and the PL change is small, similar to that in the absorbance (Fig. 2a). Comparison between the TIPS-Pn:PMMA d=2 nm sample data in the 'bottom' and 'top' configuration suggests that there are domains in this film where singlet fission occurs, leading to significant molecular populations residing in the dark  $^1(TT)/T..T$  states, but most of these molecules are in intermolecular configurations not conducive to dimerization. In contrast, most of the dark molecular populations in a more concentrated sample with d=1.3 nm are capable of dimerization.

# TMS-Tc and tBu-Tc: photophysics vs photochemistry and photoconductivity

Photodegradation measurements on encapsulated crystalline tBu- and TMS-Tc in Fig. 3 display the evolution of emissive states during photodimerization. In fresh TMS-Tc

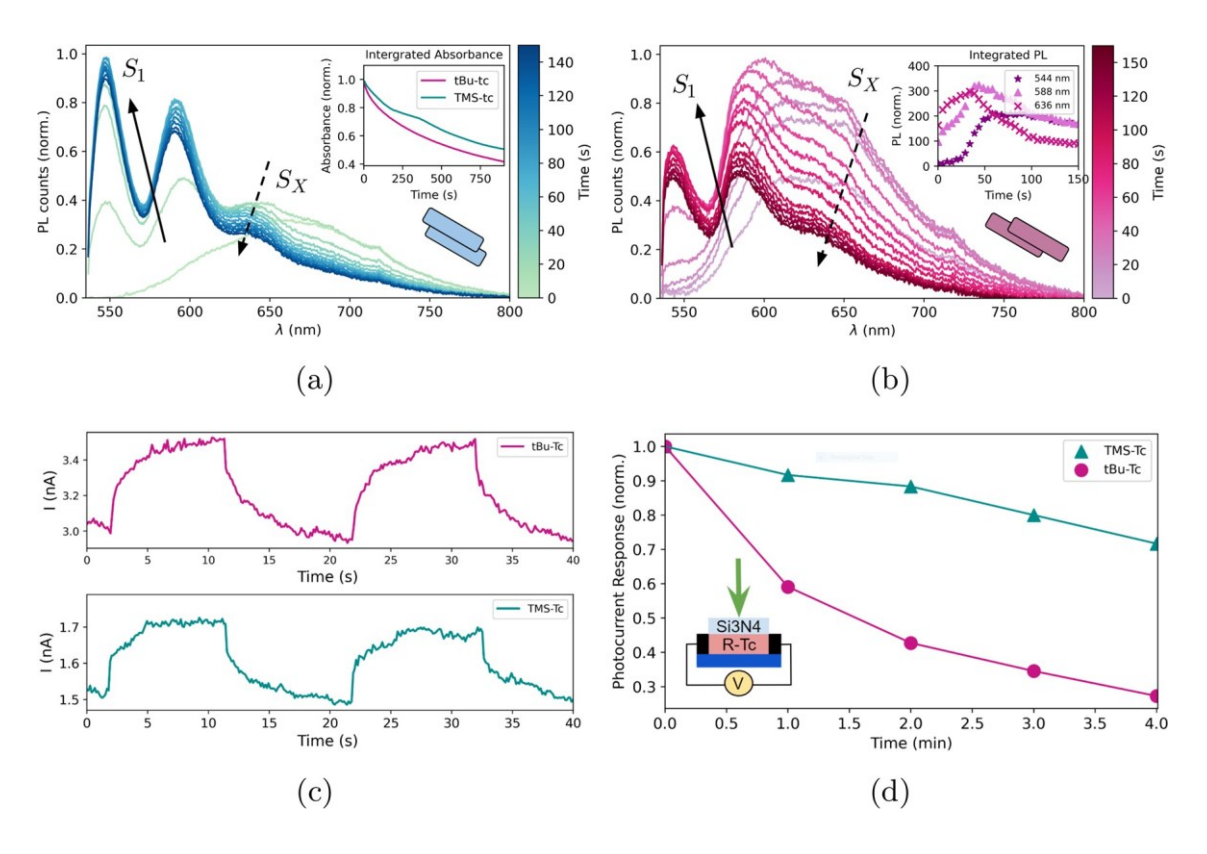


**Fig. 3** Evolution of PL spectra in **a** TMS-Tc and **b** tBu-Tc crystals during photodimerization under 532 nm cw excitation at 5 W/cm². In **a**, the initial TMS-Tc PL from a trap state Sx decreases, accompanied by a fast rise in  $S_1/S_{lagg}$  emission. Inset shows integrated  $S_0$ - $S_1$  optical absorbance decays due to dimerization for the TMS- and tBu-Tc, where tBu-Tc has a faster decay rate. Diagram in lower right depicts TMS-Tc packing motif. In **b**, the initial tBu-Tc PL from Sx increases before decreasing, while  $S_1/S_{lagg}$  emission increases. The inset tracks the PL counts at 544 nm, 588 nm, and 636 nm to show differences in

the evolution of emissive states.  $\bf c$  Photocurrent in tBu- and TMS-Tc crystals exposed to a periodic 532 nm cw excitation (200 mW/cm²) at the applied voltage of 110 V (two light on/off cycles are shown).  $\bf a$  Photocurrents obtained by subtracting the steady-state current in the dark from that under illumination, normalized by their values at  $\bf t=0$  (fresh sample) in TMS-Tc and tBu-Tc devices as the molecules undergo photodimerization under 532 nm cw illumination, showing a large photocurrent decrease in tBu-Tc, while TMS-Tc is more stable. Inset shows schematics of the measurement

and tBu-Tc samples, PL is initially dominated by a broad excimer-like emission maximized at 660 nm and 630 nm, respectively, from a trap state Sx. As TMS-Tc degrades, this Sx emission decreases in yield while there is a simultaneous increase in PL from the S<sub>1</sub>/S<sub>1agg</sub> states. In tBu-Tc, however, there is a large increase in the Sx state emission at the beginning of the measurement, followed by its decay and the eventual dominance of S<sub>1</sub>/S<sub>1agg</sub> PL (inset of Fig. 3b).

The photocurrent measures the ability of the material to photogenerate and transport charge carriers. Photocurrents measured periodically during a photodimerizationinducing continuous 532 nm illumination (Fig. 3c) show a more pronounced loss in charge generation and transport properties in tBu-Tc as compared to TMS-Tc (reaching 30% of the initial photocurrent in tBu-Tc as compared to 75% in TMS-Tc under the same conditions), a trend qualitatively consistent with a faster decay of the S<sub>0</sub>-S<sub>1</sub> absorption for the tBu-Tc as compared to that in TMS-Tc (inset of Fig. 3a) as the molecules photodimerize. No correlation in the photocurrent behavior was observed with that of PL emission. This is consistent with most of the molecules residing in dark states and emissive molecules being only a small subset of the overall population responsible for the photocurrent generation.

### **TES-Tc and TBDMS-Tc: B-field-dependent** photochemistry

The evolution of the PL spectra of TES-Tc and TBDMS-Tc crystals in vacuum due to photodimerization under 532 nm 25 W/cm<sup>2</sup> excitation are shown in Fig. 4. While TES-Tc does have some broad Sx emission at >650 nm in a fresh sample, similar to TMS- and tBu-Tc (Fig. 1d), it rapidly

(within seconds) degrades upon light exposure, after which it emits only  $S_1/S_{\rm lagg}$  PL with a vibronic progression in the 550–670 nm range, and without further spectral evolution.

Over the duration of the measurement, the total PL yield of TES-Tc increases by more than an order of magnitude, indicating that the photodimerization is efficiently disabling a nonradiative process, such as dark <sup>1</sup>(TT)/T..T states formation, which suppresses  $S_1/S_{1agg}$  PL in the fresh sample. TBDMS-Tc PL has the opposite trend, where the

photodimerization causes a small decrease in the already low initial PL from the aggregate state S<sub>lagg</sub> with a vibronic progression in the 600-700 nm range, with no evidence of accompanying increase in PL from any other emissive state. Unlike the 'slip-stack' R-Tc derivatives, TBDMS-Tc does not have an appreciable population of low-energy emissive trap states Sx.

To explore the relationship between singlet fission and photodimerization, we studied TES-Tc and TBDMS-Tc single crystals undergoing photodimerization in vacuum under magnetic fields (B-fields). In these materials, B-fields mediate singlet fission, with high B-fields impeding the separation of the <sup>1</sup>(TT) states into weakly correlated triplet pairs (T..T) and free triplets [15]. Photodimerization-induced evolution of PL spectra was measured at 0 T and 6 T B-field, with integrated PL counts for these two cases shown in the insets in Fig. 4. In both cases, the B-field induces faster photodimerization, where TES-Tc PL increases faster and TBDMS-Tc PL decreases faster. Comparison between the integrated PL time evolution at 0 T and 6 T also suggests that a larger population is susceptible to dimerization at 6 T. In particular, bi-exponential fits to the data in the insets of Fig. 4 yield a maximum PL yield increase in TES-Tc of a factor of 14 at 0 T, and 23 at 6 T. Similarly, in TBDMS-Tc

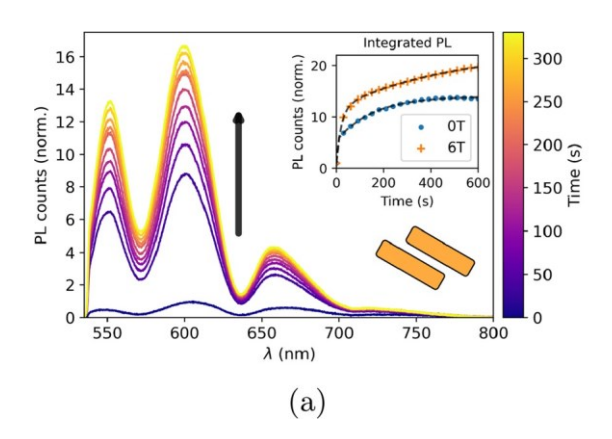
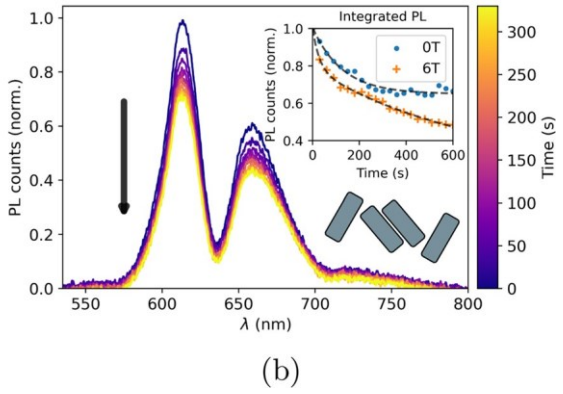


Fig. 4 Evolution of PL spectra of a) TES-Tc and b) TBDMS-Tc crystals during photodimerization induced by 532 nm cw excitation at 25 W/cm<sup>2</sup> in vacuum. Inset diagrams in the lower right depict packing motif. TES-Tc has a large increase in PL yield during photodimerization due to nonradiative processes becoming disabled, increasing PL from competitive emissive states. TBDMS-Tc instead has only a



small decrease in PL yield during photodimerization. The inset plots show integrated PL counts during photodimerization at 0 T and 6 T B-fields, and the black lines are bi-exponential fits to the decays. When <sup>1</sup>(TT) separation into T..T is impeded at 6 T, both materials undergo more pronounced photodimerization



the minimum total PL yield reached is about 0.65 at 0 T and 0.4 at 6T of the original yield at t = 0.

### **Discussion**

The effects of photodegradation on nonradiative decay processes are qualitatively similar in TIPS-Pn and R-Tc. There are two key takeaways from the photodegradation measurements: a) a large increase in PL yield from the  $S_1/S_{lagg}$  state in TIPS-Pn and R-Tc derivatives with 'slipstack' packing, which is related to the EPO (in air) and photodimer (no air) formation disabling singlet fission and b) photodimerization is enhanced in B-field.

In TIPS-Pn:PMMA films with average intermolecular spacing d = 1.3 nm, the EPO formation and photodimerization rates were found to differ by a factor of 5. This is in contrast to TIPS-Tc [14], which exhibited a factor of 650 faster EPO formation as compared to dimerization in pristine films. This difference is largely due to a considerably less efficient EPO formation in TIPS-Pn, as compared to TIPS-Tc. Type II mechanism of EPO formation in acenes, which proceeds via energy transfer from T<sub>1</sub> of the acene to the ground-state triplet oxygen followed by reactive singlet oxygen generation, is dominant in TIPS-Tc but inefficient in TIPS-Pn due to the low triplet energy (0.8 eV) of TIPS-Pn as compared to 0.98 eV necessary to sensitize singlet oxygen formation [3, 5]. Type I mechanism that relies on electron transfer from a singlet state  $S_1$ to oxygen to form a reactive superoxide, which is important for EPO formation in dilute TIPS-Pn solutions [3], could also be impeded in films because of ultrafast singlet fission depopulating the  $S_1$  state.

Analysis of photophysical properties of R-Tc derivatives is challenging due to the multitude of excited states involved and the presence of emissive low-energy trap states in most derivatives under study, which have been previously observed in similar systems such as DPH and DBP derivatives [13, 16]. In particular, crystals of three derivatives with a 'slip-stack' packing motif, but not the TBDMS-Tc with a 'sandwich-herringbone' packing motif, exhibited low-energy trap Sx emission. This may suggest that formation of trap states is promoted by large availability of -stacked molecules in dimer-like configurations. Our observation of higher affinity for dimerization of 'slipstacked' tBu-Tc, with the smallest lattice unit cell and the lowest volume of the side group R, to photodimerization (Fig. 3) supports this hypothesis. Also in tBu-Tc, the competition between populations of the dark <sup>1</sup>(TT)/T..T states and Sx is apparent via an initial increase in Sx emission (inset of Fig. 3b) as molecules in dark states dimerize and become unavailable for singlet fission.

In spite of differences in the emissive excited states and how their PL evolves during photodimerization in TES-Tc and TBDMS-Tc (PL increases in TES-Tc and decreases in TBDMS-Tc, Fig. 4), the B-field effect on the photodimerization is qualitatively similar in these two crystals: both the photodimerization rate and the number of dimerization-affected molecules increase at high B-fields. High B-fields impede the separation of the triplet pairs <sup>1</sup>(TT) into weakly correlated/uncorrelated triplet states T..T/ T<sub>1</sub> states [15]. Therefore, higher population of <sup>1</sup>(TT) would be expected, and it could increase populations in the singlet states (such as  $S_1/S_{1agg}$  or Sx). Therefore, the B-fieldenhanced photodimerization (insets of Fig. 4) suggests that molecules in the <sup>1</sup>(TT) intermediate and singlet states with populations promoted by B-field are more susceptible for photodimerization as compared to molecules in configurations favorable for separation of triplet pairs towards free triplet formation. Therefore, morphologies conducive to triplet separation [17] while avoiding parallel molecular stacks with short intermolecular spacings would both enhance singlet fission and suppress photodimerization.

### Conclusion

We have shown that photodegradation of a material can be used to understand photophysical processes impacting nonradiative relaxation such as singlet fission and to identify the nature of emissive states. Our investigation into the impact of photodegradation in TIPS-Pn and R-Tc derivatives reveals key insights into the photophysics of these singlet fission materials. Both endoperoxide formation and dimerization disable singlet fission as molecules degrade and remove nonradiative relaxation pathways, resulting in large increases in PL from the singlet states. In TIPS-Pn:PMMA films, dark <sup>1</sup>(TT)/T..T states form even in relatively dilute films, and only a minor subset of these dark molecules are in configurations susceptible to photodimerization. In more concentrated TIPS-Pn:PMMA films, we observed EPO formation and photodimerization rates differing by a factor of 5, as compared to over two orders of magnitude in TIPS-Tc [14], due to strongly suppressed EPO formation in TIPS-Pn.

Comparison of the photophysics and photochemistry of R-Tc crystals revealed significant differences in both photodimerization and singlet fission/emissive state formation behavior of derivatives with 'slip-stack' (R = tBu, TMS, TES) and 'sandwich-herringbone' (R = TBDMS) packing motifs. The 'slip-stack' packing was found to favor formation of an emissive trap state Sx and undergo photodimerization with efficiency dependent upon the intermolecular spacing. In derivatives with both 'slip-stack' and 'sandwich-herringbone' packing motifs,

suppressing triplet pair separation with strong magnetic fields shows similar decreases in photostability as more molecules reside in  $S_1/S_{1agg}/Sx$  and  $^1(TT)$  states, which promotes photodimerization.

**Author contributions** WG, MC, and MG prepared samples, collected data, and wrote the manuscript. RL fabricated encapsulated samples for dimerization studies. DW and JA synthesized the organic compounds. SP performed crystallography. OO supervised the project and edited the manuscript.

**Funding** This work was supported by the National Science Foundation (NSF CHE-1956431). The synthesis of organic semiconductors was supported by the NSF DMR (DMREF-1627428). Sample fabrication and characterization was partially performed in NSF-funded user facilities via NNCI:NNI EECS-2025489 and MRI DMR-1920368

**Data availability** Data sets generated during the current study are available from the corresponding author on reasonable request.

### **Declarations**

**Conflict of interest** The authors declare no competing interests.

### References

- 1. O. Ostroverkhova, Organic optoelectronic materials: mechanisms and applications. Chem. Rev. 116(22), 13279-13412 (2016). https://doi.org/10.1021/acs.chemrev.6b00127
- 2. M.B. Smith, J. Michl, Singlet fission. Chem. Rev. 110(11), 6891– 6936 (2010). https://doi.org/10.1021/cr1002613
- W. Fudickar, T. Linker, Why triple bonds protect acenes from oxidation and decomposition. J. Am. Chem. Soc. 134(36), 15071-15082 (2012). https://doi.org/10.1021/ja306056x
- 4. P. Coppo, S.G. Yeates, Shining light on a pentacene derivative: the role of photoinduced cycloadditions. Adv. Mat. 17(24), 3001-3005 (2005). https://doi.org/10.1002/adma.200501471
- 5. K.J. Thorley, H. Le, Y. Song, J.E. Anthony, Unravelling the major factors in photo-oxidative stability of anthradithiophene derivatives. J. Mater. Chem. C 10(42), 15861–15871 (2022). https://doi. org/10.1039/d2tc02922g
- 6. A.J. Musser, J. Clark, Triplet-pair states in organic semiconductors. Annu. Rev. Phys. Chem. 70, 323-351 (2019). https://doi.org/ 10.1146/annurev-physchem-042018-052435
- 7. A.J. Baldacchino, M.I. Collins, M.P. Nielsen, T.W. Schmidt, D.R. McCamey, M.J.Y. Tayebjee, Singlet fission photovoltaics: progress and promising pathways. Chem. Phys. Rev. 3(2), 021304 (2022). https://doi.org/10.1063/5.0080250
- 8. G. Mayonado, K.T. Vogt, J.D.B. Van Schenck, L. Zhu, G. Fregoso, J. Anthony, O. Ostroverkhova, M.W. Graham, High-symmetry anthradithiophene molecular packing motifs promote thermally activated singlet fission. J. Phys. Chem. C 126(9), 4433-4445 (2022). https://doi.org/10.1021/acs.jpcc.1c10977

- 9. J.D.B. Van Schenck, W.T. Goldthwaite, R. Puro, J.E. Anthony, O. Ostroverkhova, Exciton polaritons reveal "hidden" populations in functionalized pentacene films. J. Phys. Chem. C 125(49), 27381–27393 (2021). https://doi.org/10.1021/acs.jpcc.1c08257
- 10. J.D.B. Van Schenck, G. Mayonado, J.E. Anthony, M.W. Graham, O. Ostroverkhova, Molecular packing-dependent exciton dynamics in functionalized anthradithiophene derivatives: From solutions to crystals. J. Chem. Phys. 153(16), 164715 (2020). https:// doi.org/10.1063/5.0026072
- 11. M.J. Kendrick, A. Neunzert, M.M. Payne, B. Purushothaman, B.D. Rose, J.E. Anthony, M.M. Haley, O. Ostroverkhova, Formation of the donor-acceptor charge-transfer exciton and its contribution to charge photogeneration and recombination in small-molecule bulk heterojunctions. J. Phys. Chem. C 116(34), 18108–18116 (2012). https://doi.org/10.1021/jp305913s
- 12. J.J. Burdett, D. Gosztola, C.J. Bardeen, The dependence of singlet exciton relaxation on excitation density and temperature in polycrystalline tetracene thin films: kinetic evidence for a dark intermediate state and implications for singlet fission. J. Phys. Chem. **135**(21), 214508 (2011). https://doi.org/10.1063/1.36646
- 13. Y. Huang, I.A. Buyanova, C. Phansa, M.E. Sandoval-Salinas, D. Casanova, W.K. Myers, N.C. Greenham, A. Rao, W.M. Chen, Y. Puttisong, Competition between triplet pair formation and excimer-like recombination controls singlet fission yield. Cell. Rep. Phys. Sci. 2(2), 100339 (2021). https://doi.org/10.1016/j. xcrp.2021.100339
- 14. R. Puro, J.D.B. Van Schenck, R. Center, E.K. Holland, J.E. Anthony, O. Ostroverkhova, Exciton polariton-enhanced photodimerization of functionalized tetracene. J. Phys. Chem. C 125(49), 27072-27083 (2021). https://doi.org/10.1021/acs.jpcc.1c06881
- 15. R. Xu, C. Zhang, M. Xiao, Magnetic field effects on singlet fission dynamics. Trends Chem 4(6), 528–539 (2022). https://doi.org/10. 1016/j.trechm.2022.03.009
- 16. M. Rosenkranz, L. Graf, B. Büchner, M. Knupfer, A.A. Popov, Photoluminescence spectroscopy of dibenzopentacene singlecrystals: multiple emissive states across temperature, time, and magnetic field in a pursuit of exothermic singlet fission. J. Mater. Chem. C 11(37), 12714–12729 (2023). https://doi.org/10.1039/ d3tc01548c
- 17. H.L. Stern, A. Cheminal, S.R. Yost, K. Broch, S.L. Bayliss, K. Chen, M. Tabachnyk, K. Thorley, N. Greenham, J.M. Hodgkiss, J. Anthony, M. Head-Gordon, A.J. Musser, A. Rao, R.H. Friend, Vibronically coherent ultrafast triplet-pair formation and subsequent thermally activated dissociation control efficient endothermic singlet fission. Nat. Chem. 9(12), 1205–1212 (2017). https:// doi.org/10.1038/nchem.2856

Publisher's Note Springer Nature remains neutral with regard to jurisdictional claims in published maps and institutional affiliations.

Springer Nature or its licensor (e.g. a society or other partner) holds exclusive rights to this article under a publishing agreement with the author(s) or other rightsholder(s); author self-archiving of the accepted manuscript version of this article is solely governed by the terms of such publishing agreement and applicable law.

